MM Science Journal | www.mmscience.eu
ISSN 1803-1269 (Print) | ISSN 1805-0476 (Online)
Special Issue | HSM 2023
17th International Conference on High Speed Machining
October 25-28, 2023, Nanjing, China
DOI: 10.17973/MMSJ.2023_11_2023106

HSM2023-00015

CHATTER SUPPRESSION FOR ROBOTIC MILLING USING A NOVEL MAGNETORHEOLOGICAL FLUID ABSORBER

Maxiao Hou [a, b], Jianghai Shi [a, b], Hongrui Cao [a, b*]

[a] School of Mechanical Engineering, Xi'an Jiaotong University, Xi'an, PR China

[b] State Key Laboratory for Manufacturing Systems Engineering, Xi'an Jiaotong University, Xi'an, PR China

*Corresponding author; e-mail: chr@mail.xjtu.edu.cn

Abstract
Industrial robots are more compliant than CNC machine tools, which makes them prone to chatter during robotic milling. Chatter has slowed down the adoption or sometimes inhibited the use of robots for machining tasks. This work presents a new chatter suppression scheme by mounting a magnetorheological fluid (MRF) absorber on the spindle housing to absorb the vibration with a specific frequency range. Firstly, a Gaussian process regression (GPR) model is used to predict the modal parameters at different machining positions. Subsequently, the predicted modal parameters are employed as input to obtain the transfer matrix for chatter frequency calculation. After that, a novel MRF absorber is designed based on the controllable shear modulus of the MRF in its pre-yield region. The simulation verifies that the designed MRF absorber can suppress chatter and thus improve the surface quality of the workpiece.

Keywords:
Robotic milling, Magnetorheological fluid absorber, Chatter suppression

1 INTRODUCTION

The flexibility and low cost of industrial robots give them the potential for machining complex and large parts. However, CNC machine tools are still the backbone of machining. The main reason for this is the low stiffness of industrial robots [Verl 2019, Lin 2022], which can cause the industrial robot to chatter even at smaller milling depths [Cordes 2019]. Therefore, how to suppress the chatter of robotic milling has become an important issue in the manufacturing industry. Various passive and active control strategies have been investigated to suppress the chatter of robotic milling [Ji 2019].

Passive chatter suppression does not require external energy input and the operation is relatively simple. At present, the passive chatter suppression of robotic milling can be divided into two types: (1) Strengthening the structural stiffness properties of the robot [Wang 2009]. (2) Mounting of various types of absorbers and dampers [Guo 2016]. [Chen 2018] designed an eddy current damper mounted on the spindle housing to suppress the chatter during robotic milling by changing the dynamics of the tool tip. Eddy current dampers can only have an optimal effect at a single chatter frequency due to uncontrollable damping, stiffness, and other parameters.

Active chatter suppression can be controlled according to the machining signal, which overcomes the disadvantages of passive chatter suppression. The chatter phenomenon occurs due to high milling forces, so the milling forces can be regulated to avoid chatter by various force sensing techniques and active control strategies [Zaeh 2015]. [Chen 2019] proposed a novel intelligent end-effector for active contact force control and chatter suppression. [Nguyen 2020] designed a pose-dependent controller to suppress chatter during robotic milling. Active control strategies suppress chatter mainly by limiting milling forces, which results in low productivity. In addition, the complexity, high cost, and high energy consumption of active control prevent its practical application. In contrast, semi-active absorbers have a promising future in robotic milling chatter suppression.

Semi-active chatter suppression requires less external energy, and its absorption of chatter energy can be controlled by changing the input energy. [Lei 2019] designed a semi-active magnetorheological elastomer (MRE) absorber with adjustable stiffness at low frequencies, which was fixed to the spindle housing to absorb the vibration energy of the mode coupling chatter during robotic milling. However, there are different views on the mechanism of mode coupling chatter generation during robotic milling. [Celikag 2021] concluded that mode coupling chatter occurs mainly during the thread turning, forming, and grinding rather than milling. The experimental results also showed that the chatter frequency of the robot is still related to the spindle speed at low spindle speed, which indicates that the chatter frequency is still caused by regenerative chatter. The regenerative chatter frequency range is large only the use of MRE absorber at low frequencies to suppress chatter can not meet the practical needs. Magnetorheological fluid (MRF) has the advantages of short response time, simple structure and easy control, and is a smart material suitable for semi-active absorber [Wang 2022, Hua 2021, Dong 2021]. The application of the MRF working in the pre-yield state enables the absorber to be controlled within a wide range of frequencies, which has rarely been investigated in robotic milling. This work develops an MRF absorber with a wider absorption

frequency bandwidth to suppress chatter during robotic milling.

The remainder of this paper is organized as follows. Section 2 presents the prediction of the chatter frequency. The design of the MRF absorber is described in Section 3. Section 4 verifies the effectiveness of the MRF absorber. Finally, the conclusion is given.

2 PREDICTION OF CHATTER FREQUENCY

In this section, the modal parameters of the robotic milling system at different machining positions are predicted using the Gaussian Process Regression (GPR) model [Nguyen 2020], and then the chatter frequency is calculated by the transfer matrix.

2.1 Prediction of modal parameters

The modal parameters obtained at the discrete machining positions are used as a training set to predict the modal parameters for the remaining machining positions (Figure 1).

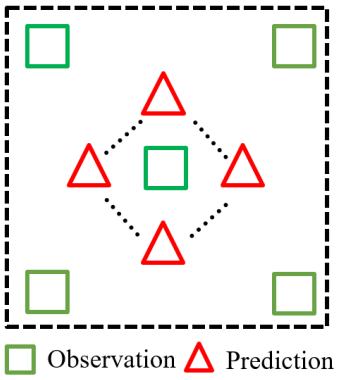

Fig. 1. Schematic of modal parameter prediction.

The modal parameters $D=\{\omega(p),\xi(p),m(p)\}$ (angular natural frequency $\omega(p)$, damping ratio $\xi(p)$, mass $m(p)$) of the machining position p are obtained using modal tests as the training set $T=(p,D)$. The prior distribution of the modal parameter D is shown below.

$$D\sim GP(\mu(p),C(p,p')+\sigma^2 I) \tag{1}$$

where $\mu(p)$ is the mean function, $C(p,p')$ is the covariance function, σ^2 is the covariance of the noise, $GP(\cdot)$ is a Gaussian distribution.

The Gaussian kernel function is as follows:

$$K(p,p')=\theta_0^2 exp\left(-\frac{(p-p')^T(p-p')}{2\theta_l^2}\right) \tag{2}$$

where θ_0 and θ_l are hyperparameters. The hyperparameters are obtained from the optimization marginal loglikelihood function [Pfrommer 1997].

$$\begin{aligned}&L(D,\theta)\\&=-\frac{\left(P-\mu(p)\right)^T(C(p,p')+\sigma^2 I)^{-1}\left(P-\mu(p)\right)}{2}\\&-\frac{log|C(p,p')+\sigma^2 I|}{2}-\frac{N log\,2\pi}{2}\end{aligned} \tag{3}$$

where $\theta=\{\theta_0,\theta_l\}$.

The modal parameters $D^*=\{\omega(p^*),\xi(p^*),m(p^*)\}$ at the machining position p^* to be predicted are shown below.

$$D^*=\mu(p^*)+C(p^*,p)(C(p,p)+\sigma^2 I)^{-1}\left(D-\mu(p)\right) \tag{4}$$

2.2 Calculation of chatter frequency

The two-degree-of-freedom robotic milling dynamics model is shown below.

$$\boldsymbol{M}\ddot{\boldsymbol{Z}}(t)+\boldsymbol{C}\dot{\boldsymbol{Z}}(t)+\boldsymbol{K}\boldsymbol{Z}(t)=\boldsymbol{F}(t) \tag{5}$$

where $\boldsymbol{Z}(t)=\begin{bmatrix}x(t)\\y(t)\end{bmatrix}$ is the displacement vector, $\boldsymbol{M}=\begin{bmatrix}m_x(p^*)&0\\0&m_y(p^*)\end{bmatrix}$, $\boldsymbol{C}=\begin{bmatrix}c_x(p^*)&0\\0&c_y(p^*)\end{bmatrix}$, $\boldsymbol{K}=\begin{bmatrix}k_x(p^*)&0\\0&k_y(p^*)\end{bmatrix}$ are the predicted mass, damping and stiffness matrices. $\boldsymbol{M}$, $\boldsymbol{C}$ and $\boldsymbol{K}$ are obtained from the predicted modal parameters. $\boldsymbol{F}(t)=\begin{bmatrix}F_x(t)\\F_y(t)\end{bmatrix}$ is the milling force [Li 2019]. The steady-state milling force has no effect on the chatter. Therefore, the steady-state milling force can be neglected and only the effect of dynamic milling forces due to regenerative effects can be analyzed.

$$\boldsymbol{F}_d(t)=\frac{a_p K_t}{2}\begin{bmatrix}h_{xx}(t)&h_{xy}(t)\\h_{yx}(t)&h_{yy}(t)\end{bmatrix}\begin{bmatrix}x(t)-x(t-\tau)\\y(t)-y(t-\tau)\end{bmatrix} \tag{6}$$

where $\boldsymbol{F}_d(t)$ is the dynamic milling force, a_p is the milling depth, K_t is the tangential milling force coefficient, $h_{xx}(t)=\sum_{j=0}^{N-1}-\left[sin2\phi_j+K_{rt}(1-cos2\phi_j)\right]g(\phi_j)$, $h_{xy}(t)=\sum_{j=0}^{N-1}-\left[(1+cos2\phi_j)+K_{rt}sin2\phi_j\right]g(\phi_j)$, $h_{yx}(t)=\sum_{j=0}^{N-1}\left[(1-cos2\phi_j)-K_{rt}sin2\phi_j\right]g(\phi_j)$, $h_{yy}(t)=\sum_{j=0}^{N-1}\left[sin2\phi_j-K_{rt}(1+cos2\phi_j)\right]g(\phi_j)$, K_{rt} is the ratio of the radial milling force coefficient to the tangential milling force coefficient, $\phi_j=\pi\Omega t/30+2\pi j/N+\phi_0$ is the instantaneous tooth position angle of the jth tool tooth. When the tool tooth j is immersed in the workpiece $g(\phi_j)$=1, otherwise $g(\phi_j)$=0. τ is the time delay.

Substituting Eq. (6) into Eq. (5), the following equation is obtained.

$$\begin{aligned}&\begin{bmatrix}\ddot{x}(t)\\\ddot{y}(t)\end{bmatrix}+\begin{bmatrix}2\xi_x(p^*)\omega_x(p^*)&0\\0&2\xi_y(p^*)\omega_y(p^*)\end{bmatrix}\begin{bmatrix}\dot{x}(t)\\\dot{y}(t)\end{bmatrix}+\\&\begin{bmatrix}\omega_x^2(p^*)&0\\0&\omega_y^2(p^*)\end{bmatrix}\begin{bmatrix}x(t)\\y(t)\end{bmatrix}=\frac{a_p K_t}{2}\begin{bmatrix}\frac{h_{xx}(t)}{m_x(p^*)}&\frac{h_{xy}(t)}{m_x(p^*)}\\\frac{h_{yx}(t)}{m_y(p^*)}&\frac{h_{yy}(t)}{m_y(p^*)}\end{bmatrix}\\&\begin{bmatrix}x(t)-x(t-\tau)\\y(t)-y(t-\tau)\end{bmatrix}\end{aligned} \tag{7}$$

where $\xi_x(p^*)$ and $\xi_y(p^*)$ are the damping ratios of the robotic milling system in the x and y directions, $\omega_x(p^*)=\sqrt{k_x(p^*)/m_x(p^*)}$ and $\omega_y(p^*)=\sqrt{k_y(p^*)/m_y(p^*)}$ are the undamped angular natural frequencies of the robotic milling system in the x and y directions.

Using the semi-discrete analysis method, the continuous time is discretized to construct a time interval $[t_i,t_{i+1}]$ $(i\in Z)$. Let $\tau=n\Delta t$, where n is the time delay term, $\Delta t=t_{i+1}-t_i$.

In the ith discrete time interval, Eq. (7) can be transformed into the following form.

$$\begin{aligned}&\begin{bmatrix}\ddot{x}(t)\\\ddot{y}(t)\end{bmatrix}+\begin{bmatrix}2\xi_x(p^*)\omega_x(p^*)&0\\0&2\xi_y(p^*)\omega_y(p^*)\end{bmatrix}\begin{bmatrix}\dot{x}(t)\\\dot{y}(t)\end{bmatrix}+\\&\begin{bmatrix}\omega_x^2(p^*)-\frac{a_p K_t h_{xxi}(t)}{2m_x(p^*)}&-\frac{a_p K_t h_{xyi}(t)}{2m_x(p^*)}\\-\frac{a_p K_t h_{yxi}(t)}{2m_y(p^*)}&\omega_y^2(p^*)-\frac{a_p K_t h_{yyi}(t)}{2m_y(p^*)}\end{bmatrix}\begin{bmatrix}x(t)\\y(t)\end{bmatrix}\\&=-\frac{a_p K_t}{2}\begin{bmatrix}\frac{h_{xxi}(t)}{m_x(p^*)}&\frac{h_{xyi}(t)}{m_x(p^*)}\\\frac{h_{yxi}(t)}{m_y(p^*)}&\frac{h_{yyi}(t)}{m_y(p^*)}\end{bmatrix}\begin{bmatrix}x_{\tau,i}\\y_{\tau,i}\end{bmatrix}\end{aligned} \tag{8}$$

where $x_{\tau,i}=w_b x_{i-n}+w_a x_{i-n+1}$, $y_{\tau,i}=w_b y_{i-n}+w_a y_{i-n+1}$, $w_a=w_b=1/2$.

According to the Cauchy transform, Eq. (8) can be rewritten as

$$\dot{\boldsymbol{z}}(t) = \boldsymbol{A}_i \boldsymbol{z}(t) + w_a \boldsymbol{B}_i \boldsymbol{z}_{i-n+1} + w_b \boldsymbol{B}_i \boldsymbol{z}_{i-n} \tag{9}$$

where

$$\boldsymbol{A}_i = \begin{bmatrix} 0 & 0 & 1 & 0 \\ 0 & 0 & 0 & 1 \\ -\omega_x^2(p^*) + \dfrac{a_p K_t h_{xxi}(t)}{2m_x(p^*)} & \dfrac{a_p K_t h_{xyi}(t)}{2m_x(p^*)} & -2\xi_x(p^*)\omega_x(p^*) & 0 \\ \dfrac{a_p K_t h_{yxi}(t)}{2m_y(p^*)} & -\omega_y^2(p^*) + \dfrac{a_p K_t h_{yyi}(t)}{2m_y(p^*)} & 0 & -2\xi_y(p^*)\omega_y(p^*) \end{bmatrix},$$

$$\boldsymbol{B}_i = -\frac{a_p K_t}{2} \begin{bmatrix} 0 & 0 & 0 & 0 \\ 0 & 0 & 0 & 0 \\ \dfrac{h_{xxi}(t)}{m_x(p^*)} & \dfrac{h_{xyi}(t)}{m_x(p^*)} & 0 & 0 \\ \dfrac{h_{yxi}(t)}{m_y(p^*)} & \dfrac{h_{yyi}(t)}{m_y(p^*)} & 0 & 0 \end{bmatrix}, \boldsymbol{z}(t) = \begin{bmatrix} x(t) \\ y(t) \\ \dot{x}(t) \\ \dot{y}(t) \end{bmatrix},$$

$\boldsymbol{z}_{i-n+1} = \boldsymbol{z}(t_{i-n+1})$, $\boldsymbol{z}_{i-n} = \boldsymbol{z}(t_{i-n})$.

Based on the zero-order hold method, Eq. (9) is discretized into the following form.

$$\boldsymbol{z}_{i+1} = \boldsymbol{P}_i \boldsymbol{z}_i + w_a \boldsymbol{R}_i \boldsymbol{z}_{i-n+1} + w_b \boldsymbol{R}_i \boldsymbol{z}_{i-n} \tag{10}$$

where $\boldsymbol{P}_i = \exp(\boldsymbol{A}_i \Delta t)$, $\boldsymbol{R}_i = (\exp(\boldsymbol{A}_i \Delta t) - \boldsymbol{I})\boldsymbol{A}_i^{-1}\boldsymbol{B}_i$.

Eq. (10) is transformed into the following form.

$$\boldsymbol{E}_{i+1} = \boldsymbol{D}_i \boldsymbol{E}_i \tag{11}$$

where $\boldsymbol{E}_i = col(x_i, y_i, \dot{x}_i, \dot{y}_i, \ldots, x_{i-n}, y_{i-n})$, $\boldsymbol{D}_i$ is composed of $\boldsymbol{P}_i$ and $\boldsymbol{R}_i$ matrices, $P_{i,cd}$ and $R_{i,cd}$ represent the elements of the cth row and dth column of the matrices $\boldsymbol{P}_i$ and $\boldsymbol{R}_i$, respectively.

$$\boldsymbol{D}_i = \begin{bmatrix} P_{i,11} & P_{i,12} & P_{i,13} & P_{i,14} & \cdots & w_b R_{i,12} & w_b R_{i,13} & w_b R_{i,14} \\ P_{i,21} & P_{i,22} & P_{i,23} & P_{i,24} & \cdots & w_b R_{i,22} & w_b R_{i,23} & w_b R_{i,24} \\ P_{i,31} & P_{i,32} & P_{i,33} & P_{i,34} & \cdots & w_b R_{i,32} & w_b R_{i,33} & w_b R_{i,34} \\ P_{i,41} & P_{i,42} & P_{i,43} & P_{i,44} & \cdots & w_b R_{i,42} & w_b R_{i,43} & w_b R_{i,44} \\ 1 & 0 & 0 & 0 & \cdots & 0 & 0 & 0 \\ \vdots & \vdots & \vdots & \vdots & \ddots & \vdots & \vdots & \vdots \\ 0 & 0 & 0 & 0 & \cdots & 0 & 0 & 0 \\ 0 & 0 & 0 & 0 & \cdots & 1 & 0 & 0 \end{bmatrix}$$

According to Eq. (11), the transfer matrix within a time delay period can be expressed as

$$\boldsymbol{\Psi} = \boldsymbol{D}_{n-1}\boldsymbol{D}_{n-2}\ldots\boldsymbol{D}_1\boldsymbol{D}_0 \tag{12}$$

The expression for the dominant chatter frequency is as follows:

$$\omega_{cq} = |\omega_{cb} + \omega_0 q| \tag{13}$$

where ω_{cq} is the dominant chatter frequency, which is related to the imaginary part of the eigenvalues of the transfer matrix $\boldsymbol{\Psi}$, ω_{cb} is base frequency, $\omega_0 = 2\pi/T$, q is the integer number, T is the tooth passing period. The detailed derivation of the chatter frequency can be found in [Dombovari 2011].

3 DEVELOPMENT OF MRF ABSORBER

Based on the predicted chatter frequency, the MRF absorber is designed in this section. MRF absorber mounted on the spindle housing to suppress the chatter generated by the robotic milling (Figure 2).

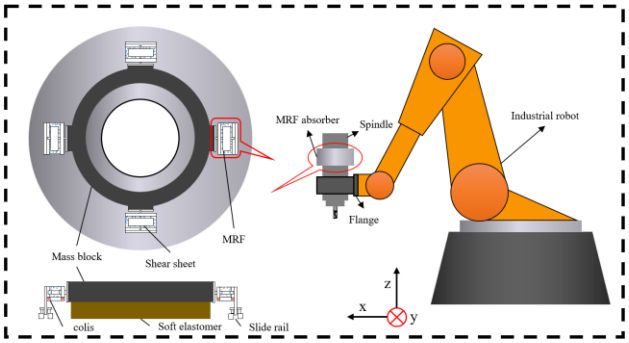

Fig. 2. Overview of MRF absorber.

The chatter frequency of robotic milling is speed dependent [Celikag 2021], which requires a wider frequency bandwidth of the absorber. The storage modulus variation percentage of MRF in the pre-yield state is much larger than MRE [Yang 2019], which can be used to design absorbers with wider frequency bandwidths. The shear mode in the proposed MRF absorber is provided by the soft elastomer and the MRF. The mass block and soft elastomer are bonded together with a cyanoacrylate glue. The shear sheet is sheared in the MRF.

The stiffness of the MRF absorber is shown below.

$$k_a = m_a(2\pi f_a)^2 \tag{14}$$

where m_a is the sum of the masses of the mass block and the shear sheet, f_a is the natural frequency of the MRF absorber.

The proposed MRF absorber (Figure 3) can have different natural frequencies by adjusting the magnetic field intensity. The natural frequency of the MRF absorber in a single direction can be expressed as

$$f_a = \frac{1}{2\pi}\sqrt{\frac{G_1 A_1}{m_a h_1} + \frac{G_2 A_2}{m_a h_2}} \tag{15}$$

where $G_1 = G_0 + (G_\infty - G_0)\left(1 - e^{-\alpha_1 B^{\alpha_2}}\right)$ is the storage modulus of the MRF, G_0, G_∞, α_1 and α_2 are empirical constants [Hirunyapruk 2008], B is the magnetic field intensity, $A_1 = 4l_1 w_1$, h_1 is the thickness of MRF, G_2 is the shear modulus of soft elastomer, $A_2 = \pi(r_2^2 - r_1^2)$, h_2 is the soft elastomer thickness.

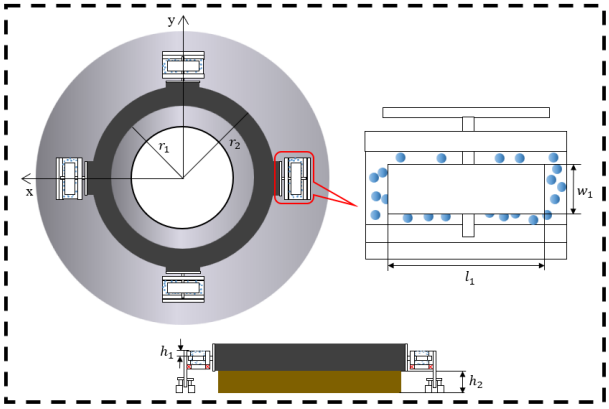

Fig. 3. Structural parameters.

4 SIMULATION ANALYSIS FOR CHATTER SUPPRESSION

According to [Hou 2023], the modal parameters of seven different machining positions are shown in Table 1.

Tab. 1. Modal parameters of robotic milling systems.

Machining positions	Natural frequency (Hz)	Modal stiffness (MN/m)	Modal damping (Ns/m)
1	18.125	0.452	264.56
2	18.125	0.504	305.29
3	18.5375	0.586	341.27
4	18.75	0.978	553.39
5	19.0625	1.06	725.11
6	19.0625	1.56	851.51
7	19.375	2.37	940.34

A schematic of the seven different machining positions of the industrial robot is shown below.

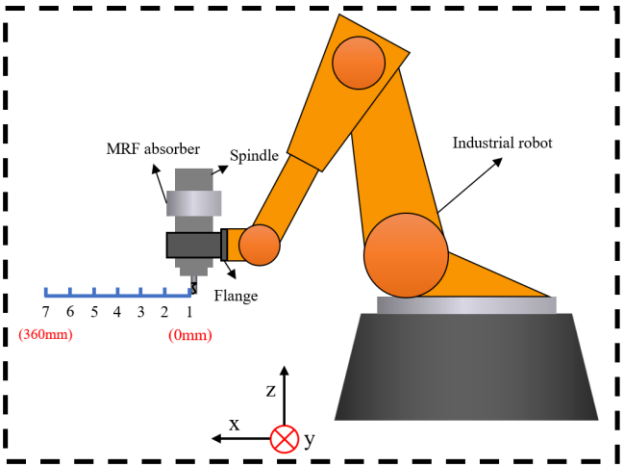

Fig. 4. Schematic diagram of machining position.

To balance the number of modal tests and the accuracy of the modal parameter predictions, the modal parameters of the 1st, 4th, and 7th machining positions are used as the training set. The comparison of the predicted and actual modal parameters is shown in Figure 5.

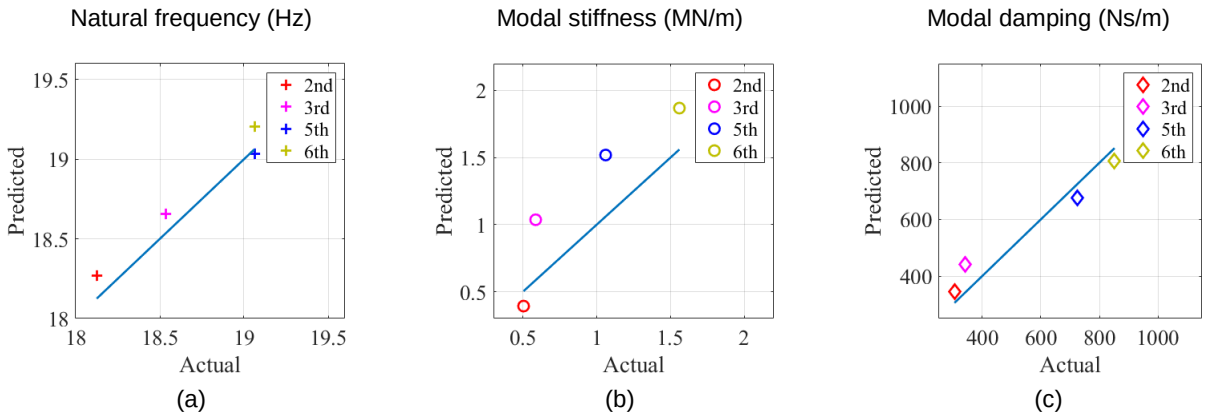

Fig. 5. Comparison of predicted and actual modal parameters.

To further illustrate the accuracy of the predicted modal parameters, the correlation coefficients (R^2) and root mean square error (RMSE) of the predicted modal parameters are shown in Table 2.

Tab. 2. Quantitative analysis of predicted modal parameter errors.

	Natural frequency (Hz)	Modal stiffness (MN/m)	Modal damping (Ns/m)
R^2	0.9864	0.9221	0.9887
RMSE	0.1173	0.3608	62.9154

Table 2 shows that the correlation coefficients of the predicted modal parameters are greater than 0.9, which has a high prediction accuracy and can be used to predict the chatter frequency.

Assume tangential milling force coefficient K_t=796 MN/m^2, normal milling force coefficient K_n=169 MN/m^2. The milling parameters are as follows: speed is 2000 r/min, milling width is 3 mm, milling tool diameter is 6 mm, number of tool teeth is 3, and sampling frequency is 25000 Hz. Then, the dominant chatter frequencies calculated from the actual and predicted modal parameters are compared as shown in Figure 6.

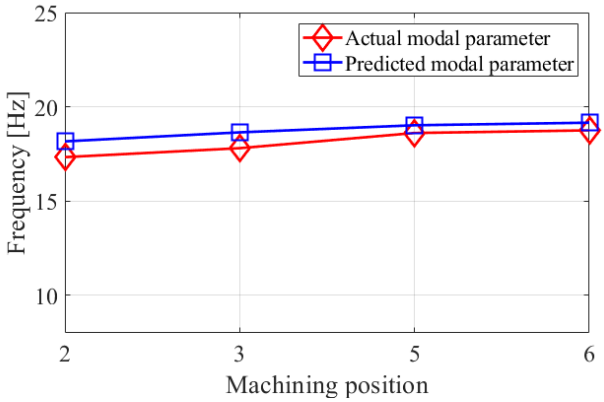

Fig. 6. Comparison of dominant chatter frequencies.

Figure 6 shows that the dominant chatter frequencies calculated using the actual and predicted modal parameters are in great agreement. The predicted chatter frequency can be used to set the natural frequencies of the MRF absorber at each machining position.

According to the practical situation, the mass block m_a=3 kg is selected. Other structural parameters are shown in Table 3.

Tab. 3. Structural parameters of MRF absorber.

Structure parameters	r_1 (m)	r_2 (m)	l_1 (m)	w_1 (m)	h_1 (m)	h_2 (m)
Values	0.1	0.15	0.04	0.018	0.02	0.05

The shear modulus of soft elastomers is in the range of 10^4 Pa [Neugebauer 2003], so the shear modulus G_2 of soft elastomers is equal to 1×10^4 Pa in this work. The parameters related to the MRF (model: GH-MRF-250, density 2.55 g/cm^3) storage modulus G_1 are shown in Table 4 [Yang 2019].

Tab. 4. The parameters related to the MRF storage modulus.

Parameters	G_0 (Pa)	G_∞ (Pa)	a_1	a_2
Values	2.51×10^3	3.5×10^6	6.8339	1.8248

Electromagnetic coils with a range of magnetic field intensity variations from 0 to 600 mT are very common on the market. Figure 7 shows the natural frequency f_a of MRF absorber in response to magnetic field intensity B.

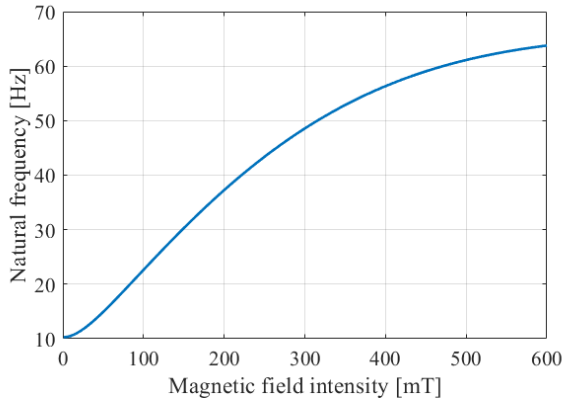

Fig. 7. The natural frequency of MRF absorber in response to magnetic field intensity.

From Figure 7, it can be seen that the designed MRF absorber has a wide range of natural frequencies to satisfy the chatter suppression requirements of robotic milling.

The modal parameters of the 5th machining position are selected to verify the effectiveness of the proposed MRF absorber. The mass and stiffness of the MRF absorber are 3 kg and 41020 N/m, respectively. The natural frequency of the absorber at the 5th machining position is the chatter frequency calculated from the predicted modal parameters. The tool tip displacements with and without MRF absorber are shown in Figures 8 and 9. Where f_c is the chatter frequency and f_t is the tooth passing frequency.

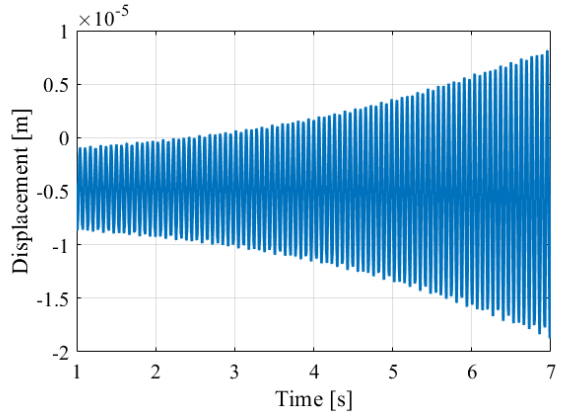

(a)

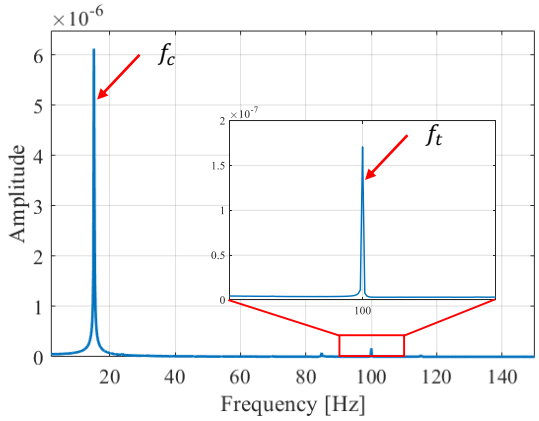

(b)

Fig. 8. Tool tip displacement without MRF absorber. (a) Time domain. (b) Frequency domain.

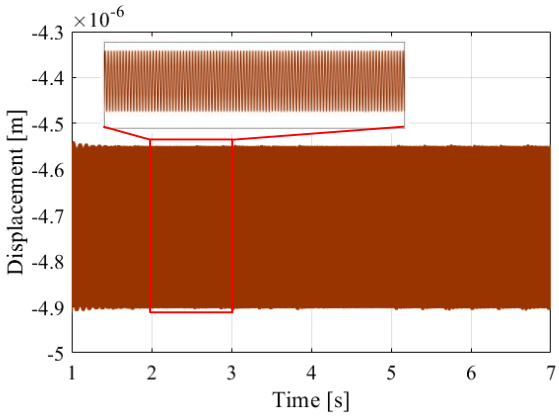

(a)

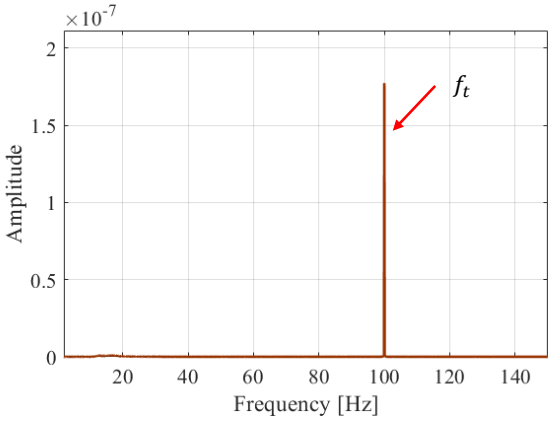

(b)

Fig. 9. Tool tip displacement with MRF absorber. (a) Time domain. (b) Frequency domain.

Figure 8 shows that the tool tip displacement without MRF absorber is unstable, and a significant chatter frequency near the natural frequency can be seen from the frequency spectrum. As can be seen from Figure 9, when the MRF absorber is mounted, the tool tip displacement is stable and the chatter frequency near the natural frequency is almost eliminated. Therefore, the proposed novel MRF absorber can set the magnetic field intensity B for each machining position in advance according to the predicted chatter frequency, which can suppress chatter during robotic milling to achieve more precise and efficient machining.

5 CONCLUSION

In this paper, a novel MRF absorber is designed to suppress chatter during robotic milling. The correlation coefficient between the predicted and actual modal parameters using the GPR model is greater than 0.9. The chatter frequency obtained with the predicted modal parameters is almost the same as the actual chatter frequency. By setting the magnetic field intensity, the natural frequency of the MRF absorber can be adjusted to match the predicted chatter frequency. Finally, it is verified by simulation that the proposed MRF absorber can suppress the chatter during the robotic milling.

Since the milling force is related to the displacement difference, directly equating the natural frequency of the MRF absorber to the predicted chatter frequency does not obtain the optimal chatter suppression performance. In the future, we will further investigate to obtain the optimal parameters of the MRF absorber and complete the experimental validation.

6 ACKNOWLEDGEMENTS

This work is supported by Aeronautical Science Foundation of China (Nos. 2022Z072070002) and National Natural Science Foundation of China (No. 52205125).

7 REFERENCES

[Verl 2019] Verl, A., Valente, A., Melkote, S., et al. Robots in machining. CIRP Annals - Manufacturing Technology, 2019, Vol.68., pp 799-822. ISSN 0007-8506

[Lin 2022] Lin, J. Z., Ye, C. C., Yang, J. X., et al. Contour error-based optimization of the end-effector pose of a 6 degree-of-freedom serial robot in milling operation. Robotics and Computer Integrated Manufacturing, 2022, Vol.73., pp 102257. ISSN 0736-5845

[Cordes 2019] Cordes, M., Hintze, W., Altintas, Y. Chatter stability in robotic milling. Robotics and Computer Integrated Manufacturing, 2019, Vol.55., pp 11-18. ISSN 0736-5845

[Ji 2019] Ji, W. and Wang, L. H. Industrial robotic machining: a review. The International Journal of the Advanced Manufacturing Technology, 2019, Vol.103., pp 1239-1255. ISSN 0268-3768

[Wang 2009] Wang, H., Zhao, W., Li, B. Dynamic analysis and robust reliability design of pan mechanism for a cooking robot. IEEE International Conference on Robotics and Biomimetics, 2009., pp 1996-2001. ISBN 978-1-4244-4774-9

[Guo 2016] Guo, Y. J., Dong, H. Y., Wang, G. F., et al. Vibration analysis and suppression in robotic boring process. International Journal of Machine Tools and Manufacture, 2016, Vol.101., pp 102-110. ISSN 0890-6955

[Chen 2018] Chen, F. and Zhao, H. Design of eddy current dampers for vibration suppression in robotic milling. Advances in Mechanical Engineering, 2018, Vol.10., pp 1-15. ISSN 1687-8132

[Zaeh 2015] Zaeh, M. F., Roesch, O. Improvement of the static and dynamic behavior of a milling robot. International Journal of Automation Technology, 2015, Vol.9., pp 129-133. ISSN 1881-7629

[Chen 2019] Chen, F., Zhao, H., Li, D. W., et al. Contact force control and vibration suppression in robotic polishing with a smart end effector. Robotics and Computer Integrated Manufacturing, 2019, Vol.57., pp 391-403. ISSN 0736-5845

[Nguyen 2020] Nguyen, V., Johnson, J., Melkote, S. Active vibration suppression in robotic milling using optimal control. International Journal of Machine Tools and Manufacture, 2020, Vol.152., pp 103541. ISSN 0890-6955

[Lei 2019] Lei, Y., Sun, S. S., Pan, Z. X., et al. Mode coupling chatter suppression for robotic machining using semi-active magnetorheological elastomers absorber. Mechanical Systems and Signal Processing, 2019, Vol.117., pp 221-237. ISSN 0888-3270

[Celikag 2021] Celikag, H., Ozturk, E., Sims, N. D. Can mode coupling chatter happen in milling? International Journal of Machine Tools and Manufacture, 2021, Vol.165., pp 103738. ISSN 0890-6955

[Wang 2022] Wang, J., Liu, Y. F., Qin, Z. Y., et al. Dynamic Performance of a novel integral magnetorheological damper-rotor system. Mechanical Systems and Signal Processing, 2022, Vol.172., pp 109004. ISSN 0888-3270

[Hua 2021] Hua, D., Liu, X., Li, Z., et al. A review on structural configurations of magnetorheological fluid based devices reported in 2018–2020. Frontiers in Materials, 2021, Vol.24. ISSN 2296-8016

[Dong 2021] Dong, B. P. and Ricles, J. M. Simplified seismic design procedure for steel MRF structure with nonlinear viscous dampers. Journal of Construational Steel Research, 2021, Vol.185., pp 106857. ISSN 0143-974X

[Pfrommer 1997] Pfrommer, B. G., Cote, M., Louie, S. G., Cohen, M. L. Relaxation of crystals with the quasi-Newton method. Journal of Computational Physics, 1997, Vol.131., pp 233–240. ISSN 0021-9991

[Li 2019] Li, D. H., Cao, H. R., Liu, J. X., et al. Milling chatter control based on asymmetric stiffness. International Journal of Machine Tools and Manufacture, 2019, Vol.147., pp 103458. ISSN 0890-6955

[Dombovari 2011] Dombovari, Z., Iglesias, A., Zatarain, M., et al. Prediction of multiple dominant chatter frequencies in milling processes. International Journal of Machine Tools and Manufacture, 2011, Vol.51., pp 457-464. ISSN 0890-6955

[Yang 2019] Yang, J., Sun, S. S., Ning, D., et al. Development and evaluation of a highly adaptive MRF-based absorber with a large effective frequency range. Smart Materials and Structures, 2019, Vol.28., pp 1-10. ISSN 0964-1726

[Hirunyapruk 2008] Hirunyapruk, C., et al. Modelling and experimental characterization of a tunable magnetorheological fluid vibration absorber. The 7th European Conference on Structural Dynamics, 2008.

[Hou 2023] Hou, M. X., Cao, H. R., Luo Y., et al. Pose-Dependent Cutting Force Identification for Robotic Milling. Journal of Manufacturing Science and Engineering, 2023, Vol.145. ISSN 1087-1357

[Neugebauer 2003] Neugebauer, D., Zhang, Y., Pakula, T., Sheiko, S. S., Matyjaszewski, K. Densely-Grafted and Double-Grafted PEO Brushes via ATRP. A Route to Soft Elastomers. Macromolecules, 2003, Vol.36., pp 6746-6755. ISSN 0024-9297